Mon. Not. R. Astron. Soc. **000**, 000–000 (1999) Printed 17 December 2007 (MN LATEX style file v1.4)

X-ray observations of low-power radio galaxies from the B2 catalogue

C. M. Canosa[1], D. M. Worrall[1,2], M. J. Hardcastle[1] and M. Birkinshaw[1,2]
[1] *Department of Physics, University of Bristol, Tyndall Avenue, Bristol, BS8 1TL*
[2] *Harvard-Smithsonian Center for Astrophysics, 60 Garden Street, Cambridge, MA 02138, U.S.A.*

17 December 2007

ABSTRACT

We present an analysis of X-ray data, taken with *ROSAT*, for a well defined sample of low-power radio galaxies from the Bologna B2 catalogue. Where possible, the HRI has been used in order to take advantage of the higher spatial resolution provided by this instrument. A variety of models are fitted to radial profiles in order to separate the resolved and unresolved X-ray emission from the galaxies. We demonstrate a strong, approximately linear, correlation between the luminosities of the unresolved X-ray components and the 5-GHz luminosities of the radio cores in this sample. This suggests a physical relationship between the soft X-ray emission of radio galaxies and the jet-generated radio core emission. We infer a nuclear jet-related origin for at least some of the X-ray emission.

Key words: galaxies: active – galaxies: clusters: general – X-rays: galaxies.

1 INTRODUCTION

It is widely accepted that the radio emission in BL Lac objects is dominated by synchrotron radiation from a relativistic jet pointed towards the observer, thus explaining, among other things, the superluminal velocities and rapid variability observed in several objects. Such a favourable orientation to the observer should not be common, implying the presence of a population of double radio sources whose twin jets lie in the plane of the sky. Low-power radio galaxies can be found which match BL Lac objects in extended radio power (Wardle, Moore & Angel 1984) and galaxy magnitude (Ulrich 1989). There is evidence that the total soft X-ray luminosity in such galaxies is correlated with the radio-core luminosity, implying a nuclear jet-related origin for at least some of the X-ray emission (Fabbiano et al. 1984). High spatial resolution X-ray measurements have further strengthened this argument by separating point-like emission from hot X-ray emitting atmospheres (Worrall & Birkinshaw 1994; Edge & Röttgering 1995; Feretti et al. 1995; Worrall 1997; Hardcastle & Worrall 1999). What has been lacking is high-resolution X-ray observations of a large unbiased sample of low-power radio galaxies with which to investigate the association of unresolved X-ray emission with the nuclear radio jet.

The B2 bright sample of radio galaxies are Bologna Catalogue 408-MHz radio sources identified with elliptical galaxies brighter than m_{Zwicky}=15.4 (Colla et al. 1975, Ulrich 1989). The radio survey occupies 0.84 steradian, and is complete at 408 MHz down to 0.2 Jy for (B1950) declinations between 29 and 34 degrees, 0.25 Jy for declinations between 24 and 29.5 degrees and between 34 and 40 degrees, and 0.5 Jy between 21.4 and 24 degrees (Colla et al. 1970, 1975; Ulrich 1989), although none of the bright sample radio galaxies lies in the last declination range. The sample comprises 50 galaxies, of which 47 are at $z \leq 0.065$ (see Table 1). The high Galactic latitudes imply a relatively small Galactic neutral hydrogen column density and small resultant X-ray absorption. The B2 sample has been shown to be well matched with radio-selected BL Lac objects in their extended radio properties and galaxy magnitudes (Ulrich 1989). In this paper we present *ROSAT* X-ray measurements of 40 galaxies which constitute an unbiased subsample of the 47 galaxies at $z \leq 0.065$. The data were taken from our pointed observations or from data in the *ROSAT* public archives.

Section 2 discusses the sample of galaxies observed with *ROSAT* and the general properties of the X-ray data. Details of our analysis and notes on some of the sources are in section 3. Section 4 describes X-ray – radio comparisons. Section 5 contains our conclusions.

A Friedmann cosmological model with $H_0 = 50$ km s^{-1} Mpc^{-1}, $q_0 = 0$ is used throughout this paper.

2 X-RAY DATA

Table 1 lists the sample of 50 B2 radio sources associated with elliptical galaxies; we have not included B2 1101+38 and B2 1652+39 as these are the well known BL Lac objects Mkn 421 and Mkn 501. We tabulate the pointed observations taken with *ROSAT* using the instrument with the highest spatial resolution, the High Resolution Imager (HRI; David et al. 1997), or, if no HRI observations were made, the Position Sensitive Proportional Counter (PSPC; Trümper 1983; Pfeffermann et al. 1987). Where multiple observations exist, we present results for the longest on-axis viewings, concentrating where possible on HRI data. Most observations result in a detection. In some cases where good data exist from the HRI and PSPC, both were analysed and compared (this was the case for B2 0055+30, 0120+33, 0149+35, 1122+39; 1217+29 and 2335+26). Within the same ROR, some HRI observations were split into observing periods about 6 months or a year apart. Where this was the case, the data have been merged after the individual 'observations' were checked for anomalies. In many cases resolved X-ray emission (measured better with the PSPC) is seen in addition to point-like emission. Complementary work discussing the extended X-ray emission and X-ray spectra of B2 radio galaxies based on PSPC observations can be found in Worrall & Birkinshaw (in preparation). Our treatment of the resolved emission in this paper is restricted to modelling it sufficiently well to determine a best estimate for the contribution from central unresolved emission.

40 of the full sample of 50 B2 radio galaxies (and the 47 at z <0.065) listed in Table 1 were observed with *ROSAT*: the demise of the satellite in early 1999 prevented observation of the remaining 7 objects with z <0.065. No known bias was introduced into the set of 40 objects for which we have data by the process of prioritizing sources for *ROSAT* observation. This is illustrated in Fig. 5, which shows histograms of 1.4-GHz extended radio power ($P_{\rm ext}$), redshift, and absolute visual magnitude ($M_{\rm v}$) for the 47 galaxies at $z \leq 0.065$. $P_{\rm ext}$ and $M_{\rm v}$ are indicators of isotropic unbeamed emission used to support the association of these galaxies with the hosts of BL Lac objects. A Kolmogorov-Smirnov test finds no significant (>90 per cent confidence) difference between the distributions of sources for which we have *ROSAT* data, and those for which we do not, in any of the quantities $P_{\rm ext}$, z, or $M_{\rm v}$.

The *ROSAT* HRI has a roughly square field of view with 38 arcmin on a side. A functional form for the azimuthally averaged point spread function (PSF) can be found in David et al. (1997). The core of the HRI radial profile of a point-like source may be wider than the nominal PSF, and ellipsoidal images are sometimes seen, due to a blurring attributable to residual errors in the aspect correction. The major axes of such ellipsoidal images are not aligned with the satellite wobble direction (the wobble is employed to ensure that no sources are imaged only in hot pixels in the HRI or hidden behind the PSPC window-support structure) and depend unpredictably on the day of observation and therefore the satellite roll angle. The asymmetry is strongest between 5 arcsec and 10 arcsec from the centroid of the image. The PSF for the HRI begins to be noticeably influenced by the off-axis blur of the X-ray telescope at $\gtrsim$7 arcmin off-axis. All HRI observations discussed here are essentially on axis.

The *ROSAT* PSPC has a circular field of view, of diameter 2 degrees, and the PSF has a FWHM of about 30 arcsec at the center of the field, degrading only marginally out to off-axis angles of about 20 arcmin. At larger radii the mirror blur dominates the spatial resolution, and at 40 arcmin off axis the FWHM of the PSF is about 100 arcsec. Only one of the 40 sources discussed here (B2 0722+30) is significantly affected by mirror blur, as all others were observed in the central part of the field of view.

We used the Post Reduction Off-Line Software (PROS; Worrall et al. 1992) to generate radial profiles of the X-ray data. Background was taken from a source-centered annulus of radii given in Table 3. Where the radial profile has been used to probe the extended emission, the contribution from extended-emission models to the background region is taken into account (Worrall & Birkinshaw 1994).

We excluded confusing sources, defined as those separated from the target by $\gtrsim$ 15 arcsec (HRI) and $\gtrsim$ 30 arcsec (PSPC), showing up at $\sim 3\sigma$ above the background level and overlapping the on-source or background regions (or being slightly beyond, but still affecting the background due to the broad wings of the PSF). Optical images (e.g the Palomar Sky Survey plates, digitized by the Space Telescope Science Institute) and radio maps were overlaid on the X-ray images, to check the identity of each target source and any neighbouring X-ray sources, and to help to classify and limit further the effects of confusing sources.

Our luminosity determination for unresolved emission assumes a power-law spectrum with an energy index α of 0.8 ($f_\nu \propto \nu^{-\alpha}$) modified by Galactic absorption. Variations in spectral form affect the luminosity, but this is normally a small error compared with statistical uncertainties.

3 RADIAL PROFILES AND NUCLEAR X-RAY EMISSION

We analyse the structure of an X-ray source by extracting a radial profile and fitting various models convolved with the energy-weighted PSF of the detector in question [the nominal PSF for the HRI (David et al. 1997) and the PSF for the PSPC (Belloni, Hasinger & Izzo 1994)].

As well as point-source models, we have fitted our radial profiles with β models (Sarazin 1986) which describe gas in hydrostatic equilibrium. The values used for β were 0.3, 0.35, 0.4, 0.5, 0.67, 0.75 and 0.9. For each source the models used are (a) point source, (b) β model and (c) point source + β model. Model parameters for sources where an extended component is detected are given in Table 2. In most cases we find that for observations with enough counts a significantly better fit to the data is achieved by fitting the composite model (c) rather than either (a) or (b) individually (see Table 2).

Residual errors in aspect correction affect the HRI PSF and must be taken into account when evaluating the contribution from a point source [see Worrall et al. (1999), where it was found that a point source can appear more like a β model with a core radius of up to about 5 arcsec (dependent on β assumed) because of the aspect smearing]. Of the sources in this paper only 1833+32 has high enough count rate to perform the dewobbling procedure described by Harris et al. (1998); we find no substantial difference in

the best-fit parameters after dewobbling. For observations where the data show extension on small scales, it is difficult to decide whether the source is really point like or indeed slightly extended. In some cases, the fit to the point+β model has a substantially lower χ^2 than the beta-model fit alone, and here we regard the point-like component as well measured. Where χ^2 remains unchanged for these two models, the total counts have been taken as an upper limit on the point-source counts. A literature search into the environments of the sources and a cross-correlation of the HRI and PSPC results, where possible, helps us further validate our HRI findings and place limits on the likelihood of the source being primarily point-like.

In the 7 cases where there are not enough counts to perform adequate radial-profile fitting , the total counts are taken as an upper limit to the contribution of point-like emission. For non-detections a 3σ upper limit, derived by applying Poisson statistics to a 5 by 5 arcsec detection cell for the HRI on-axis observations (3 cases), and a 120 by 120 arcsec detection cell for the PSPC observation of the off-axis source B2 0722+30, centred on the position of the radio and optical core, is taken as an upper limit on both the total and the unresolved X-ray emission.

Table 2 gives results for the 16 sources with enough counts to allow radial-profile model fitting. Table 3 presents the net counts within a circle of specified radius and, for the sources with enough counts to allow radial profiling (consisting of a minimum of ∼70 counts over 3 data bins), the point-source contribution. There is a wide range in the ratio of unresolved to resolved counts. X-ray core flux and luminosity densities calculated from the unresolved count rates, and radio core flux and luminosity densities taken from the literature are given in Table 4.

3.1 Notes on individual sources

Where analysis of sample sources is present in the literature, comparisons have been made with the results presented here. Results for B2 0055+26 are taken from Worrall, Birkinshaw & Cameron (1995). B2 0326+39, 1040+31 and 1855+37 are discussed in detail in Worrall & Birkinshaw (in preparation). The HRI results for B2 2229+39 are consistent with the findings of Hardcastle, Worrall & Birkinshaw (1998), for a PSPC observation of the source.

B2 0120+33

Identified with the galaxy NGC 507, the source lies in Zwicky cluster 0107+3212 and is one of the brightest galaxies in a very dense region. Extended X-ray emission is seen out to a radius of at least 16 arcmin, and there is evidence for the presence of a cooling flow and possible undetected cooling clumps distributed at large radii (Kim & Fabbiano 1995). B2 0120+33 has a steep radio spectrum and weak core. It may be a source with particularly weak jets, or possibly a remnant of a radio galaxy whose nuclear engine is almost inactive and whose luminosity has decreased due to synchrotron or adiabatic losses (Fanti et al. 1987).

The HRI map shows the central region of this source to be asymmetrical, with a large extended emission region to the SW. Radial-profile fitting of the innermost parts of this galaxy with point, β, and point+β models, show that a good fit to the data is achieved by using a single β model with β=0.67, which gives a core radius of $4''$. The β+point model gives a marginally better fit, but the additional component is not significant on an F-test at the 90% confidence level. Therefore, we have taken the total counts from the inner regions of this source as an upper limit on any unresolved emission present, keeping in mind that this may also include a cooling-flow contribution (this also holds for other sources with possible unresolved cooling flows such as B2 0149+35, 1346+26 and 1626+39).

B2 0149+35

B2 0149+35 is identified with NGC 708 and is associated with the brightest galaxy in the cluster Abell 262. Braine & Dupraz (1994) suggest that it contains a cooling flow which may contribute excess central X-rays, and this may explain why B2 0149+35 has a higher point-like X-ray luminosity and flux than expected based on other sample members. It is not possible to separate spatially a cooling-flow contribution from unresolved X-ray emission using the PSPC observation, and the asymmetry of the source makes the extraction of a radial profile difficult.

The HRI observation is split up into 2 OBIs (Observation Intervals), one of which shows a barred N-S structure. Each OBI was individually analysed by taking close-in source regions, and this gives results which are consistent with the PSPC data from the inner region of B2 0149+35. In the longer, and more reliable, of the two OBIs (12.7ks), 207 counts were detected. The point-like contribution to the net emission from this source however, is not significant at the 95 per cent level when an F-test is performed. The detected counts are therefore taken as an upper limit on the point model emission. The shorter OBI was not used.

B2 0207+38

This source is described as being more similar to an S0 or to a spiral galaxy than an elliptical (Parma et al. 1986). It has also been called a post-eruptive Sa (Zwicky et al., 1968) or a distorted Sa (de Vaucouleurs, de Vaucouleurs & Corwin 1975). The radio structure is disc-like and there is no sign of either a radio core, or of jets or radio lobes (Parma et al. 1986). It is probably a starburst, like B2 1318+34. There are no *ROSAT* X-ray data for this source.

B2 0836+29A

This object (4C 29.30), this object has been often confused in the literature with the cD galaxy B2 0836+29 at z=0.079, which is the brightest galaxy in Abell 690.

B2 0924+30

B2 0924+30 appears to be a remnant radio galaxy whose nuclear engine is inactive (Fanti et al., 1987; Cordey 1987; Giovannini et al. 1988). It is the brightest member in a Zwicky cluster (Ekers et al. 1981), and the X-ray data suggest extended X-ray emission, although the detection is of marginal significance. The relatively high X-ray emission for a source with no detectable core radio emission may therefore be due to the extended gas in the cluster. We have taken the detected emission as an upper limit on possible point source emission.

B2 1122+39

Analysis of this source, both in the PSPC and in the HRI, shows that ∼3 per cent of the total emission is contributed by an unresolved source. This is consistent with the findings of Massaglia et al. (1996) who find a contribution from a point source of <6 per cent.

B2 1217+29

PSPC and HRI analysis of this source are consistent. A

β+point model fits the data better than a β model alone (see Table 2).

B2 1254+27

There is a large discrepancy between the positions given for this object in the NASA Extragalactic Database (NED) and the SIMBAD Astronomical Database. This is because the radio source has, in some cases, been incorrectly associated with the galaxy NGC 4819 rather than the true host galaxy for the radio emission which is NGC 4839.

NGC 4839 is classified confusingly as morphological type S0 (Eskridge & Pooge 1991), E/S0 (Jorgensen, Franx & Kjaegaard 1992) or as a cD (Gonzalez-Serrano, Carballo & Perez-Fournon 1993; Fisher, Illingworth & Franx 1995). Andreon et al. (1996) also mention that the low average surface brightness suggests that this galaxy is dominated by an extended disc. The X-ray map of the source shows extended large scale emission to the SW [described by Dow & White (1995), as being in the process of interacting with the intracluster medium of the main (Coma) cluster]. This goes beyond the size of the optical galaxy and has been excluded here so as not to affect the background emission. About 88 per cent of the net counts arise from a point-like emission component.

B2 1257+28

The region of enhanced X-ray emission in B2 1257+28 in the Coma cluster is substantially smaller than the size of the optical galaxy. Small on-source (12 arcsec radius) and background (15-22.5 arcsec) source-centered circles were used in order to verify the contribution from unresolved X-ray emission given by our best-fit model.

B2 1317+33

B2 1317+33 (NGC 5098A) has a companion galaxy (NGC 5098B) at a distance of ~ 40 arcsec. We have checked that the X-ray and radio source come from NGC 5098A by overlaying the radio, optical and X-ray maps.

B2 1318+34

B2 1318+34 is a classic merger-induced starburst, whose total radio flux can be attributed to starburst activity rather than an active nucleus (Condon, Huang & Yin 1991).

B2 1346+26

The source is a cD galaxy in Abell 1795, identified with 4C 26.42. It contains a central cooling-flow component, as discussed in Fabian et al. (1994). *HST* WFPC2 images of the core of this cooling flow are presented in Pinkney et al. (1996).

Our analysis of the HRI data detects a central point source which is significant on an F-test at the 95 per cent confidence level (see Table 2). About 1 per cent of the total counts lie in this point-like component (see Table 3).

B2 1422+26

B2 1422+26 is not radially symmetric in the X-ray. An off-axis X-ray source in the same field of view gives a good fit to the nominal PSF, and so we can rule out the possibility that the X-ray extension seen in B2 1422+26 is due to the *ROSAT* aspect correction problem. The possible detection of a point-like component is not significant on an F-test at the 95 per cent level (although it passes at the 90 per cent level). We have nevertheless taken the point counts calculated from these model fits as our best estimate of the central emission, though the errors are large.

B2 1615+35

HRI analysis is consistent with Feretti et al. (1995). The X-ray emission is largely point like (see Table 3), with $\sim$60 per cent of the net counts coming from the point source.

B2 1621+38

B2 1621+38 was analysed by Feretti et al. (1995), who found a point-source contribution of $\leq$50 per cent of the total X-ray flux. Our analysis is consistent with this result; we find the point-source contribution to be 18$\pm$4 per cent.

B2 1626+39

B2 1626+39 lies in a cluster (A2199), with a prototypical cooling flow. Owen & Eilek (1998) conclude that the radio source is relatively young and has been disrupted by the surrounding gas. The *ROSAT* HRI data set for this source consists of 2 OBIs roughly 7 months apart. Only in the second observation does the source appear extended, with two adjacent peaks. We have taken this to be due to errors in the aspect correction or processing effects and therefore have used only the first OBI in our analysis.

B2 1833+32

B2 1833+32 is an FRII radio galaxy (Laing, Riley & Longair 1983; Black et al. 1992) with broad emission lines (Osterbrock, Koski & Phillips 1975; Tadhunter, Perez & Fosbury 1986; Kaastra, Kunieda & Awaki 1991). Its higher than expected X-ray flux, as compared with the core radio strength, may arise from emission in the central accretion disc around the active nucleus, seen due to an advantageous viewing angle as indicated by the broad emission lines.

B2 2236+35

This source has a double symmetric radio jet embedded in a low surface-brightness region. The two extended lobes are similar in strength and size (Morganti et al. 1987). The X-ray emission at radii greater than about 20 arcsec seems aligned with the radio jets in this source. Model fitting shows $\sim$25 per cent of the total counts to be in the point source.

4 X-RAY – RADIO COMPARISONS

In Table 3 we list the net counts detected for each source within a specified radius and our best estimate of the contribution from unresolved emission derived as described above. 1-keV luminosity densities and broad-band soft X-ray luminosities calculated from the values for unresolved emission are given in Table 4, along with the radio core flux density and luminosity density. In Fig. 2 we show a logarithmic plot of radio core luminosity density against the unresolved core X-ray emission; the corresponding flux density-flux density plot appears in Fig. 3.

Both the logarithmic X-ray and radio flux densities and the corresponding luminosities are correlated at the $>$ 99.99 per cent significance level on a modified Kendall's τ-test which takes upper limits into account, as implemented in ASURV (Lavalley, Isobe & Feigelson 1992). The flux-flux correlation gives us confidence that the luminosity-luminosity relationship is not an artificially-introduced redshift effect.

To determine the slope of the core flux-flux and luminosity-luminosity plots, a generalised version of the Theil-Sen estimator was used as presented in Akritas, Murphy & LaValley (1995). This takes into account the nature of the upper limits by assuming that the individual points are all part of the same parent population. For more details of this analysis and its advantages over the more

commonly used survival-analysis method, see Hardcastle & Worrall (1999), where it is explained how using the bisector of two regression lines provides a more robust estimate of the slope. This method however does not give a value for the intercept of the best-fit line. To determine the best-fit line plotted on Fig. 2, a regression based on the bisector of slopes determined by the Schmitt algorithm as implemented in ASURV was used, because it does allow us to determine an intercept.

For the whole sample, the Theil-Sen luminosity-luminosity slope is 1.05 with 90 per cent confidence limits 0.86-1.28. There are however, a few galaxies that should be removed. These are the starburst object B2 1318+34 (which is not member of a strict AGN sample), and the FRII B2 1833+32 (which is a broad-line galaxy). For comparison purposes we have retained these objects on Figs. 2 & 3. With the omission of these two sources, we find a Theil-Sen slope of 0.96 for the luminosity-luminosity relation, with a 90 per cent confidence range (derived from simulation) of 0.78 – 1.21. The median logarithmic dispersion about the regression line is ~ 0.2. Schmitt regression analysis of the slope gives consistent results, with a slope of 1.15 and a 90 per cent confidence limit of 0.92 – 1.39. Normalisation of the Schmitt slope at a radio luminosity of 10^{22}W Hz^{-1}sr^{-1}, gives the best-fit normalisation value of 15.55 (i.e. the predicted X-ray flux at that radio luminosity is $10^{15.55}$W Hz^{-1}sr^{-1}. The 90 per cent confidence range on this is 15.2 to 15.9.

From combining statistical methods, the best overall estimate and 90 per cent confidence uncertainty for the core X-ray–radio luminosity relation for low-power radio galaxies is given by:

$$\log(l_x) = (0.96^{+0.25}_{-0.18}) \log (l_r/10^{22}) + (15.55 \pm 0.35)$$

A couple of sources lie significantly away from the regression line (B2 1254+27 and B2 1257+28). Both lie in the Coma cluster and may be contaminated by cluster emission.

B2 0120+33 has been classified as a possible remnant of a radio galaxy whose nuclear engine is inactive (Fanti et al. 1987), and is shown as an upper limit above the expected value based on the X-ray correlation for other sample members. Its high total X-ray flux may be due to the cooling flow seen by Kim & Fabbiano (1995) (see Section 3 of this paper) and makes the extraction of the core flux difficult. B2 0924+30 is also a relic source. B2 0149+35 contains a cooling flow which may contribute excess central X-rays (Braine & Dupraz 1994).

The correlation shown in Figs. 2 & 3 suggests a physical relationship between the soft X-ray emission of radio galaxies and the jet-generated radio core emission. Correlations between the total X-ray emission and the radio core emission have been seen in the *Einstein Observatory* data (e.g Fabbiano et al. 1984), but did not have the spatial resolution necessary to separate point and extended components. Our *ROSAT* analysis and the decomposition of the X-ray emission into resolved and unresolved components, now shows that the nuclear X-ray emission is strongly correlated with the nuclear radio-core emission. This favours models which imply a nuclear jet-related origin for at least some of the X-ray emission.

5 CONCLUSIONS

Radial profiling and model fitting of *ROSAT* data, primarily from the HRI, have allowed us to separate point-like contributions from the overall X-ray emission in low power radio galaxies from a well defined, nearby sample. We find flux-flux and luminosity-luminosity core X-ray/radio correlations for such sources, with slopes that are consistent with unity. This suggests a physical relationship between the soft X-ray emission of radio galaxies and the jet-generated radio core emission, with the clear implication that at least some of the X-ray emission is related to the nuclear radio jet. In future work we will estimate X-ray beaming parameters under the assumption that radio galaxies are the parent population of BL Lac objects.

ACKNOWLEDGMENTS

This research has made use of the NASA/IPAC Extragalactic Database (NED) which is operated by the Jet Propulsion Laboratory, California Institute of Technology, under contract with the National Aeronautics and Space Administration. Support from NASA grant NAG 5-1882 is gratefully acknowledged. We thank the referee for useful comments.

REFERENCES

Akritas M.G., Murphy S.A., LaValley M.P., 1995, J. American Statistical Association, 429, 171
Andreon S., Davoust E., Michard R., Nieto J.-L., Poulain P., 1996, A&AS, 116, 429
Belloni T., Hasinger G., Izzo C., 1994, A & A, 283, 1037
Black A.R.S., Baum S.A., Leahy J.P., Perley R.A., Riley J.M., Scheuer P.A.G., 1992, MNRAS, 256, 186
Braine J., Dupraz C., 1994, A&A, 283, 407
Bridle A.H., Fomalont E.B., Cornwell T.J., 1981, AJ, 86, 1294
Bridle A.H., Baum S.A., Fomalont E.B., Parma P., Fanti R., Ekers R.D., 1991, A&A, 245, 371
Colla G., et al., 1970, A&AS 1, 281
Colla G., Fanti C., Fanti R., Gioia I., Lari C., Lequeux J., Lucas, R., Ulrich, M.H, 1975, A&AS, 20, 1
Condon J.J., Huang Z.-P., Yin Q.F., 1991, ApJ, 378, 65
Cordey R., 1987, MNRAS, 227, 695
David L.P., Harnden F.R, Kearns K.E., Zombeck M.V., 1997, U.S. ROSAT Science Data Center report, available at http://hea-www.harvard.edu/rosat/rsdc-www/hricalrep.html
Dow K.L., White S.D.M., 1995, ApJ, 439, 113
Edge A.C., Röttgering H., 1995, MNRAS, 277, 1580
Ekers R.D., 1978, A&A, 69, 253
Ekers R.D., Fanti R., Lari C., Parma P., 1981, A&A, 101, 194
Eskridge P.B., Pooge R.W., 1991, AJ, 101, 2056
Fabbiano G., Trinchieri G., Elvis M., Miller L., Longair M., 1984, ApJ, 277, 115
Fabian A.C., Arnaud K.A., Bautz M.W., Tawara Y., 1994, ApJ, 436, L63
Fanti R., Gioia I., Lari C., Lequeux J., Lucas R., 1973, A&A, 24, 69
Fanti R., Lari C., Parma P., Bridle A.H., Ekers R.D., Fomalont E.B., 1982, A&A, 110, 169
Fanti C., Fanti R., De Ruiter H.R., Parma P., 1987, A&AS, 69, 57
Feretti L., Giovannini G., 1985, A&A, 147, L13
Feretti L., Fanti R., Parma P., Massaglia S., Trussoni E., Brinkmann W., 1995, A&A, 298, 699

Fisher D., Illingworth G., Franx M., 1995, ApJ, 438, 539
Giovannini G., Feretti L., Gregorini L., Parma P., 1988, A&A, 199, 73
Giovannini, Feretti and Comoretto, 1990, ApJ, 358, 159
Gonzalez-Serrano J.I., Carballo R., Perez-Fournon I., 1993, AJ, 105, 1710
Hardcastle M.J., Worrall D.M., 1999, MNRAS, submitted
Hardcastle M.J., Worrall D.M., Birkinshaw, M., 1998, MNRAS, 296, 1098
Harris D.E., Silverman J.D., Hasinger G., Lehmann I., 1998, A&AS, 133, 431
Johnston K.J., et al.,1995, AJ, 110, 880
Jorgensen I., Franx M., Kjaegaard P., 1992, A&AS, 95, 489
Kaastra J.S., Kunieda H., Awaki H., 1991, A&A, 242, 27
Kim K-T., 1994, A&AS, 105, 403
Kim D-W., Fabbiano G., 1995, ApJ, 441, 182
Laing R.A., Riley J.M., Longair M.S., 1983, MNRAS, 204, 151
Laing R.A., 1996, in Energy Transport in Radio Galaxies and Quasars, p246, ASP Conference Series, vol. 100
Lavalley, M., Isobe, T., Feigelson, E., 1992, Astronomical Data Analysis Software and Systems I, A.S.P. Conference Series, Vol. 25, 1992, D. M. Worrall, C. Biemesderfer, and J. Barnes, eds., p. 245.
Massaglia S., Trussoni E., Caucino S., Fanti R., Feretti L., Parma P., Brinkmann W., 1996, A&A, 309, 75
Morganti R., Fanti C., Fanti R., Parma P., ,de Ruiter H.R. 1987, A&A, 183, 203
Osterbrock D.E., Koski A.T., Phillips M.M., 1975, ApJ, 197, L41
Owen F.N., Eilek J.A., 1998, ApJ, 493, 73
Parma P., De Ruiter H.R., Fanti C., Fanti R., 1986, A&AS, 64, 135
Pfeffermann E., et al., 1987, in Soft X-ray Optics & Technology, ed. E.-E Koch & G. Schmahl, Proc. SPIE, 733, 519
Pinkney, J., et al., 1996, ApJ, 468, L13
Sarazin C.L., 1986, Rev. Mod. Phys., 58, 1
Schilizzi R.T., Fanti C., Fanti R., Parma P., 1983, A&A, 126, 412
Stark A.A., Gammie C.F., Wilson R.W., Bally J., Linke R.A., Heiles C., Hurwitz M, 1992, ApJS, 79, 77
Stocke J.T., Burns J.O., 1987, ApJ, 319, 671
Tadhunter C.N., Perez E., Fosbury R.A.E., 1986, MNRAS, 219, 555
Trümper J., 1983, Adv. Space Res., 2, 241
Ulrich M.-H., 1989, in BL Lac Objects, eds. L. Maraschi, T. Maccacaro & M.-H. Ulrich, Springer, Berlin, p. 45
de Vaucouleurs G., de Vaucouleurs A., Corwin Jr. H., 1975, Second Reference Catalogue of Bright Galaxies, University of Texas Press, Austin
Venturi T., Giovannini G., Feretti L., Comoretto G., Wehrle A.E. 1993, ApJ, 408, 81
Venturi T., Castaldini C., Cotton W.D., Feretti L., Giovannini G., Lara L., Marcaide J.M., Wehrle A.E., 1995, ApJ, 454, 735
Wardle J.F.C., Moore R.L., Angel J.R.P., 1984, ApJ, 279, 93
Worrall D.M., 1997, in Relativistic Jets in AGNs, eds. M. Ostrowski, M. Sikora, G. Madejski, M. Begelman, Astronomical Observatory of the Jagiellonian University, Krakow, p. 20
Worrall D.M., Birkinshaw M., 1994, ApJ, 427, 134
Worrall D.M., et al., 1992, in Data Analysis in Astronomy IV, ed. V. Di Gesu et al., Plenum, New York, p. 145
Worrall D.M., Birkinshaw M., Cameron R.A., 1995, ApJ, 449, 93
Worrall D.M., Birkinshaw M., Remillard R.A., Prestwich A. Tucker W.H., Tananbaum H., 1999, ApJ, 516, 163
Zwicky F., et al., 1968, Catalogue of Galaxies and of Clusters of Galaxies vol. 4., California Institute of Technology Press

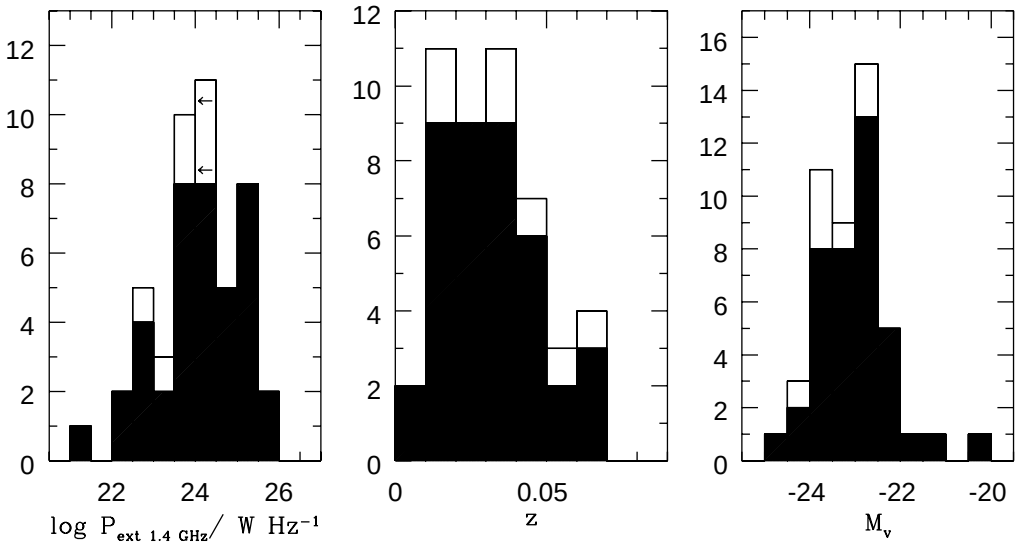

Figure 1. Histograms of extended radio power at 1.4 GHz, redshift and galaxy V-band magnitude for the 47 B2 $z \leq 0.065$ sources (Ulrich 1989). Solid shading shows the 40 sources for which we have *ROSAT* X-ray data.

Table 1. Data on the 50 B2 sample galaxies. RA and DEC are given for the radio core where possible, and the optical identification otherwise (optical positions are labelled with a *). References are as follows: 1, Fanti et al. (1987), 2, Worrall et al. (1995); 3, Ekers (1978); 4, Fanti et al. (1982); 5, Bridle et al. (1991); 6, Measured from radio map in Laing (1996); 7, Johnston et al. (1995), 8, Measured from radio maps supplied by L. Rudnick; 9, Venturi et al. (1995); 10, Stocke & Burns (1987); 11, Fanti et al. (1973); 12, Schillizzi et al. (1983), 13, Kim (1994); 14, Bridle et al. (1981); 15, Giovannini et al. (1988); 16, Estimated from map of Venturi et al. (1993). Galactic absorbing column density $N_{\rm H}$ is taken from Stark et al. (1992). Redshifts are from Colla et al. (1975). $M_{\rm v}$ is the absolute visual magnitude of the host galaxy from Ulrich (1989). The ROR is the *ROSAT* observational request number, with 'rh' referring to HRI observations and 'rp' to PSPC observations. Offset refers to the off-axis angle, and is shown only for those sources with offsets $\geq$6 arcmin. A dash in the last three columns indicates no observation.

B2 name	Other name	RA (J2000)	DEC (J2000)	Ref.	$N_{\rm H}$ (10^{20} cm^{-2})	z	$M_{\rm v}$	ROR	Livetime (s)	Offset (arcmin)
0034+25		00 37 5.50	+25 41 56.4	1	3.84	0.0321	−22.95	–	–	–
0055+30	NGC315	00 57 48	+30 21 08	16	5.77	0.0167	−23.68	rh701308n00	14821	–
0055+26	NGC326	00 58 22.63	+26 51 58.8	2	5.47	0.0472	−23.78	rp700884n00	20356	–
0104+32	3C31	01 07 24.9	+32 24 45.00	6	5.53	0.0169	−22.60	rh600496n00	24815	–
0116+31	4C31.04	01 19 35.0	+32 10 50	7	5.82	0.0592	−23.50	–	–	–
0120+33	NGC507	01 23 39.99	+33 15 21	1	5.41	0.0164	−23.14	rh600680n00	27992	–
0149+35	NGC708	01 52 46.46	+36 09 06.6	1	5.30	0.0160	−21.70	rh800870n00	12715	–
0206+35	4C35.03	02 09 38.55	+35 47 51.1	1	5.90	0.0375	−23.34	rh701564n00	21408	–
0207+38	NGC828	02 10 09.7	+39 11 30 *	1	5.36	0.0181	−23.58	–	–	–
0222+36		02 25 27.34	+37 10 27.8	1	5.19	0.0327	−22.80	rh704037n00	28701	–
0258+35	NGC1167	03 01 42.4	+35 12 20	1	9.26	0.016	−22.30	rh704039n00	18992	–
0326+39		03 29 23.9	+39 47 32	5	14.21	0.0243	−22.50	rp701442n00	18931	–
0331+39	4C39.12	03 34 18.42	+39 21 24.3	1	14.60	0.0202	−22.88	rh701832n00	25993	–
0648+27		06 52 02.51	+27 27 39	1	12.23	0.0409	−24.03	–	–	–
0722+30		07 25 37.26	+29 57 14.8	1	6.48	0.0191	−21.28	rp200450n00	11362	28.0
0755+37	NGC2484	07 58 28.18	+37 47 12.5	1	5.02	0.0413	−23.50	rh701309n00	19509	–
0800+24		08 03 16.6	+24 40 34	10	4.30	0.0433	−22.98	rh702077n00	29936	–
0836+29A	4C29.30	08 40 02.35	+29 49 02.2	1	4.11	0.0650	−23.88	rh800159	19036	–
0844+31	4C31.32	08 47 59.02	+31 47 09	1	3.45	0.0675	−24.15	–	–	–
0915+32		09 18 59.4	+31 51 40.4	1	1.86	0.0620	−23.98	–	–	–
0924+30		09 28 52.8	+29 59 07 *	11	1.88	0.0266	−22.88	rh701831	28722	–
1040+31	4C29.41	10 43 19	+31 31 01	1	1.82	0.036	−22.58	rp700883n00	21248	–
1102+30		11 05 22.81	+30 09 41.5	1	1.98	0.0720	−24.08	–	–	–
1108+27	NGC3563	11 11 25.20	+26 57 48.8	1	1.66	0.0331	−23.28	–	–	–
1113+29	A1213	11 16 34.5	+29 15 16	1	1.57	0.0489	−23.70	rp800167	6547	6.5
1122+39	NGC3665	11 24 43.5	+38 45 47	1	2.08	0.0067	−22.55	rh701938	24971	–
1144+35		11 47 22.1	+35 01 07.3	1	1.81	0.0630	−23.40	rh700862	3000	–
1217+29	NGC4278	12 20 06.82	+29 16 50.5	12	1.75	0.0021	−20.38	rh701004a01	5810	–
1254+27	NGC4839	12 57 24.37	+27 29 52.7	1	0.90	0.02464	−23.48	rp800009n00	19713	7.5
1256+28	NGC4869	12 59 21.3	+27 54 40.3	13	0.91	0.0224	−22.13	rh800242a04	36932	6.9
1257+28	NGC4874	12 59 35.7	+27 57 33	1	0.91	0.0239	−23.20	rh800242a04	36932	–
1317+33	NGC5098	13 20 14.72	+33 08 36.0	1	1.03	0.0379	−23.30	rh800696n00	18908	–
1318+34		13 20 35.3	+34 08 22	1	0.99	0.0232	−22.32	rh704040n00	22510	–
1321+31	NGC5127	13 23 45.00	+31 33 55.7	4	1.16	0.0161	−22.42	rh701829a01	21781	–
1322+36	NGC5141	13 24 51.43	+36 22 42.8	1	0.96	0.0175	−22.51	rh702076n00	35078	–
1346+26	A1795	13 48 52.6	+26 35 35 *	1	1.12	0.0633	−24.03	rh800222a01	10966	–
1350+31	3C293	13 52 17.83	+31 26 46.3	14	1.29	0.0452	−23.06	rh700366	6136	–
1422+26		14 24 40.51	+26 37 30.5	1	1.61	0.0370	−22.63	rh701830	31329	–
1525+29	A2079	15 27 44.40	+28 55 6.5	15	2.38	0.0653	−24.20	–	–	–
1553+24		15 56 03.90	+24 26 52.9	1	4.42	0.0426	−23.13	rh701565	39080	–
1610+29	NGC6086	16 12 36.7	+29 29 16 *	1	3.10	0.0313	−22.90	rh800650n00	45547	–
1615+35	NGC6109	16 17 40.50	+35 00 14.7	3	1.47	0.0296	−22.85	rh800164n00	33399	–
1621+38	NGC6137	16 23 03.11	+37 55 20.2	1	1.09	0.031	−23.60	rh800165n00	31560	–
1626+39	3C338	16 28 38.22	+39 33 04.1	1	0.88	0.0303	−23.80	rh800429a01	20755	–
1833+32	3C382	18 35 03	+32 41 47	1	7.28	0.0586	−24.20	rh700368	4943	–
1855+37		18 57 37.5	+38 00 33 *	1	8.01	0.0552	−24.50	rp701445n00	8771	–
2116+26		21 18 33.0	+26 26 49.4	1	9.65	0.0164	−22.59	–	–	–
2229+39	3C449	22 31 20.575	+39 21 29.76	8	11.05	0.0171	−22.18	rh704035n00	19064	–
2236+35		22 38 29.41	+35 19 47.0	1	8.60	0.0277	−22.70	rh702075	30971	–
2335+26	3C465	23 35 58.97	+26 45 16.16	9	4.91	0.0301	−23.85	rh800715	61933	–

Table 2. Results of model fits. Sources with too few counts to perform a radial fitting, or those where the more complicated models show no improvement over the simple point-source model, are not given. Sources where the β+point model fails an F-test for improvement over a β model at the 95 per cent confidence level are denoted with a * . If these sources then have a small value for the core radius in the beta model, all the counts are assigned to the point source, otherwise the β+point counts are used as a best estimate of the central point-like emission.

B2	Point source		β model				β+point model			
name	χ^2	df	β	θ_{core} (arcsec)	χ^2	df	β	θ_{core} (arcsec)	χ^2	df
0055+26	9780	11	0.9	254	43	10	0.9	267	9.4	9
0326+39	1474	41	0.35	0.05	70	39	0.35	60	44	38
1040+31	2173	41	0.35	0.05	42	39	0.35	28	34	38
1122+39	707	10	0.67	20	4.8	9	0.75	25	4.6 *	8
1217+29	8.4	9	0.67	1.0	4.3	8	0.9	10	2.3	7
1254+27	22	9	0.5	5.0	4.3	9	0.9	37.0	3.8 *	8
1257+28	522	7	0.5	102	6.0	6	0.5	290	0.38	5
1317+33	2464	30	0.5	8	27	29	0.5	10	25 *	28
1346+26	7734	31	0.67	46	303	30	0.5	28	48	29
1422+26	1300	10	0.5	33	7.6	9	0.5	47	4.7 *	8
1615+35	4.1	5	0.5	$<$1.0	1.7	4	0.75	69	0.069	3
1621+38	330	9	0.5	6	11	8	0.5	12	8.2 *	7
1626+39	39840	96	0.3	7	77	95	0.3	9	73	94
1855+37	6714	41	0.35	35	54	39	0.4	70	32	38
2229+39	4102	11	0.9	275	14	10	0.9	282	4.0	9
2236+35	89	11	0.67	4.8	11	10	0.75	10	8.4 *	9

Table 3. Net counts within the given source radius and the estimated contribution from unresolved emission (point counts). Sources marked with an asterisk lie in cluster environments, so the net counts are more dependent on the radii chosen for source and background regions than for field galaxies. Details of any foreign sources excluded from these regions are not shown. Consult Table 1 to see if counts are for the HRI or PSPC. All PSPC counts are from the range 0.2-1.9 keV only, where the PSF is well modelled. Note: For B2 0055+26, counts and radii quoted are for position angles 125-290 degrees only, due to the asymmetry of the source. 'Bkg radii' shows the inner and outer background radii.

B2 name	Net counts	Error	Point model counts	Error	Percentage of counts in point source	Source radius (arcsec)	Bkg radii (arcsec)	
0055+30	284	22	284	22	100	50	50	256
0055+26	1066	42	60	10	6	120	120	256
0104+32 *	165	17	165	17	100	30	60	256
0120+33 *	245	27	<245	–	–	30	45	60
0149+35 *	207	23	<207	–	–	20	20	35
0206+35 *	63	10	63	10	100	15	60	256
0222+36	32	14	<32	–	–	30	50	128
0258+35	20.9	9.6	<20.9	–	–			
0326+39	638	56	134	14	21	180	180	340
0331+39	462	39	462	39	100	100	100	500
0722+30	<69	–	<69	–	–			
0755+37	177	19	177	19	100	45	45	256
0800+24	<10	–	<10	–	–			
0836+29A *	<8	–	<8	–	–			
0924+30	75	29	<75	–	–	32	32	36
1040+31	942	82	139	17	15	180	180	340
1113+29 *	26	15	26	15	100	75	75	256
1122+39	159	22	4.1	6.8	3	50	100	256
1144+35	71	11	71	11	100	50	50	256
1217+29	104	14	86	14	82	50	50	256
1254+27 *	267	71	236	55	88	50	50	120
1256+28 *	<12	–	<12	–	–			
1257+28 *	219	44	34	14	15	45	60	120
1317+33	531	31	20	12	4	60	60	256
1318+34	11	11	<11	–	–	30	128	256
1321+31 *	48	20	<48	–	–	50	60	128
1322+36	54	27	<54	–	–	50	50	90
1346+26 *	11590	150	61	19	1	256	256	360
1350+31	20.7	9.5	<20.7	–	–	50	50	256
1422+26	254	42	18.8	6.6	7	100	200	256
1553+24	122	24	122	24	100	50	50	256
1610+29 *	69	17	69	17	100	30	100	256
1615+35	102	22	62	11	61	50	50	256
1621+38	440	29	77	15	18	50	50	256
1626+39 *	3516	77	59	22	2	45	60	120
1833+32	2913	56	2913	56	100	45	60	120
1855+37	1191	83	75	13	6	180	180	340
2229+39	301	56	24.5	7.6	8	150	325	375
2236+35	160	34	40	12	25	75	75	250
2335+26 *	439	40	439	40	100	60	100	256

Table 4. Radio and X-ray core flux densities and luminosities. For the radio core, references are as follows: 1, Giovannini et. al (1990); 2, Fanti et al. (1987); 3, Venturi et al. (1993); 4, Fomalont, private communication; 5, various, see text; 6, measured from maps supplied by R. Morganti. A source of type U is undetected in the X-ray, and the X-ray measurement is a 3σ upper limit. In a source of type P a compact source is detected in the X-ray, and all the X-ray counts are attributed to the X-ray core. In type R, a mixture of extended and compact X-ray emission is found. The X-ray core value is from the best-fit point-source contribution to a multi-component model. Sources of type L are upper limits corresponding to the total detected counts on a source, either because there are too few counts to perform an adequate radial profile fit or because the source has complicated structure which is not well characterised by our models. $L_{\rm point}^{0.2-2.5{\rm keV}}$ is the estimated luminosity of the X-ray point-like component between 0.2 and 2.5 keV. The X-ray values assume a power-law spectrum with energy index 0.8, and errors in the 1 keV luminosity density are statistical only.

B2 name	$S_{\rm core}^{\rm 5GHz}$ (mJy)	Ref.	$L_{\rm core}^{\rm 5GHz}$ (10^{20} W Hz^{-1} sr^{-1})	$S_{\rm point}^{\rm 1keV}$ (nJ)	$L_{\rm point}^{\rm 1keV}$ (10^{15} W Hz^{-1} sr^{-1})	$L^{0.2-2.5}$ (10^{35} W)	Type
0055+30	450	3	430	190	18 ± 1	1.3	P
0055+26	8.6	4	66	11	8.5 ± 1	0.62	R
0104+32	92	1	90	64	6.3 ± 0.7	0.46	P
0120+33	1.4	1	1.3	<83	<7.8	<0.56	L
0149+35	5	1	4	<59	<5.2	<0.38	L
0206+35	106	1	510	29	14 ± 2	1.0	P
0222+36	90	1	330	<10	<4	<0.3	L
0258+35	<15	1	<13	<10	<1	<0.08	L
0326+39	70	1	140	36	7.3 ± 0.8	0.53	R
0331+39	125	1	175	230	33 ± 3	2.4	P
0722+30	51	1	64	<20	<3	<0.2	U
0755+37	190	1	1110	85	51 ± 5	3.7	P
0800+24	3	1	20	<3	<2	<0.1	U
0836+29A	8.2	1	120	<4	<6	<0.4	U
0924+30	<0.4	1	<1.00	<20	<5	<0.3	L
1040+31	55	1	240	16	7.5 ± 0.9	0.55	R
1113+29	41	1	340	10	8 ± 5	0.6	P
1122+39	6	1	0.9	1	0.02 ± 0.03	0.001	R
1144+35	250	1	3400	170	240 ± 40	18	P
1217+29	350	1	5.28	100	0.16 ± 0.03	0.011	R
1254+27	2.3	5	4.8	25	5.2 ± 1	0.38	R
1256+28	2	1	3	<2	<0.3	<0.03	U
1257+28	1.1	1	2.2	6	1 ± 0.4	0.08	R
1317+33	8	6	40	7	3 ± 2	0.2	R
1318+34	84	5	150	<3	<0.6	<0.04	L
1321+31	21	1	19	<10	<1	<0.09	L
1322+36	75	1	79	<10	<1	<0.07	L
1346+26	53	1	730	36	52 ± 20	3.7	R
1350+31	100	1	700	<20	<20	<1	L
1422+26	25	1	120	4	2 ± 0.7	0.1	R
1553+24	53.6	2	333	11	6.8 ± 1	0.49	P
1610+29	<6	1	<20	12	4.3 ± 1	0.31	P
1615+35	28	1	84	13	3.9 ± 0.7	0.28	R
1621+38	50	1	160	16	5.3 ± 1	0.38	R
1626+39	100	1	314	20	6 ± 2	0.4	R
1833+32	190	1	2240	6090	7500 ± 100	543	P
1855+37	<100	1	<1040	35	38 ± 7	2.8	R
2229+39	37	1	37	15	1.5 ± 0.5	0.11	R
2236+35	8	1	20	14	3.7 ± 1	0.27	R
2335+26	230	1	713	66	21 ± 2	1.5	P

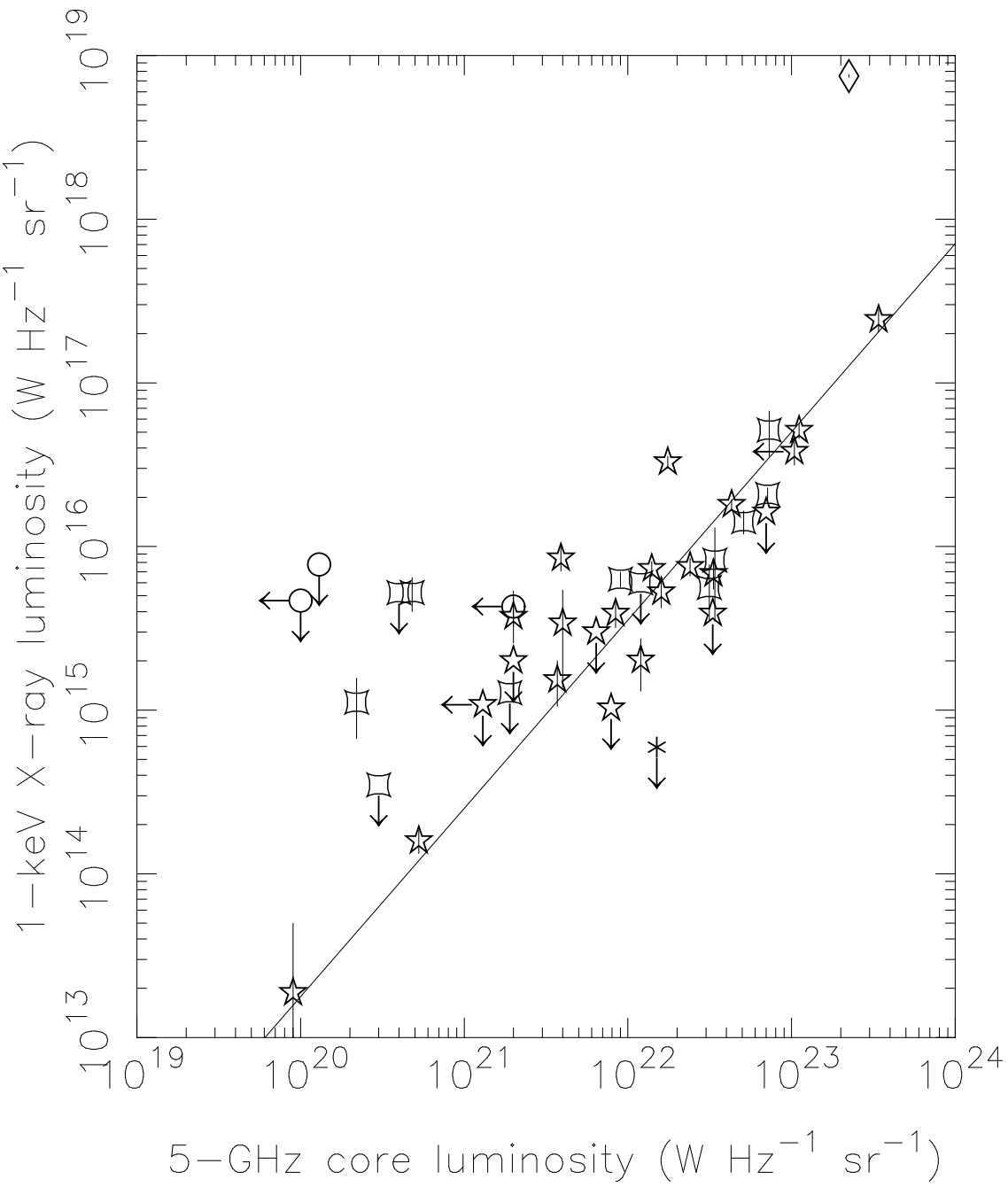

Figure 2. X-ray core luminosity is plotted vs radio core luminosity. The line drawn is derived from the Schmitt regression [(excluding a broad-line radio galaxy and a starburst galaxy (see text)] and has a slope of 1.15 and an intercept of -9.82. Cluster sources are shown by squashed squares, an open circle denotes a relic source, a cross represents a starburst galaxy, and a closed star is everything else. The excluded broad line FRII source 3C382 has been displayed as a diamond; it is over-bright in X-rays for its core-radio strength, suggesting an additional X-ray emission component, consistent with unified models. The arrows show where upper limits have been taken and in all other cases 1σ error bars are shown.

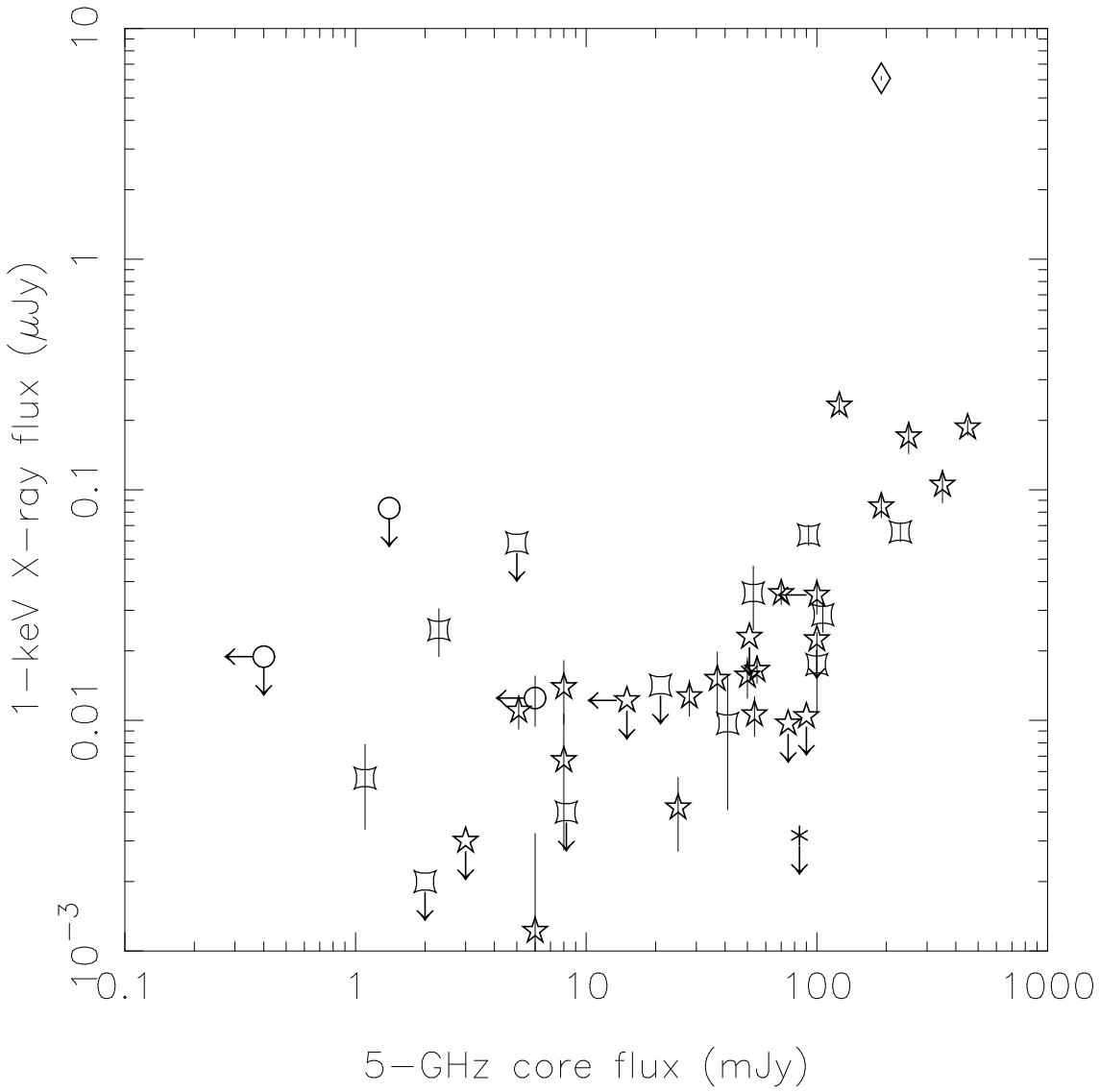

Figure 3. X-ray against radio flux density. Symbols as for Fig. 2. The correlation persists here, and is significant at the >99.99 level.